Director-Configurational Transitions around Microbubbles of Hydrostatically Regulated Size in Liquid Crystals[*)]

液晶に分散したマイクロバブルの静水圧によるサイズ制御とダイレクタの配向転移

産業技術総合研究所ナノテクノロジー研究部門
科学技術振興機構 ERATO/SORST 液晶ナノシステム
横山　浩

When particles are suspended in a liquid crystal matrix, in which elongated molecules are aligned along a common direction called the director, long-range interparticle forces mediated by elastic deformations of the director field emerge [1–5]. Because of this nonclassical interparticle interaction, colloidal particles in nematic liquids spontaneously form a rich variety of ordered structures such as linear chains [6,7] or two-dimensional lattices [8,9]. Possible applications of these soft ordered structures are currently being explored, for example, as a tunable photonic crystal [10]. For a spherical particle immersed in a uniformly aligned nematic liquid crystal with a strong homeotropic alignment at the particle-liquid crystal interface, two distinct director configurations are possible depending on the particle size as shown in Fig. 1: a hyperbolic hedgehog configuration [11–13], consisting of a -1 pointlike defect located on one side of the polar axis of the particle, and a Saturn-ring [14,15] configuration that literally involves a -1/2 line defect around the equator of the particle. The hyperbolic hedgehog structure, being asymmetrical about the equator plane, yields a long-range orientational distortion that is dipolar in nature. The Saturn-ring configuration, on the other hand, is symmetrical about the equator, thereby making it quadrupolar. The detailed energetics of the hyperbolic hedgehog and Saturn-ring configurations has been theoretically studied, along with the interparticle forces giving rise to the multiparticle clusters [14–18], and predicted the existence of a configurational transition from one state to the other as the particle size is changed [4,5].

So far, however, the experimental investigations to test the particle-size-induced transition have been hampered by the invariability of the particle size [19]. In this Letter, a high-pressure technique will be introduced to overcome these limitations. We use a nematic liquid crystal host into which micrometer-sized gas bubbles are injected, and, by applying a hydrostatic pressure, the diameter of these gas bubbles is continuously varied. We demonstrate the transition from a dipolar hyperbolic hedgehog configuration to a quadrupolar Saturn-ring con-figuration, as predicted theoretically, when the particle size is continuously decreased.

The nematic liquid crystal (4-pentyl-4’-cyanobiphenyl:5CB) is sandwiched in a parallel cell consisting of two circular glass plates (30 mm ϕ, thickness 2 mm), the internal surfaces of which are coated with a planar aligning agent. The two glass plates are glued

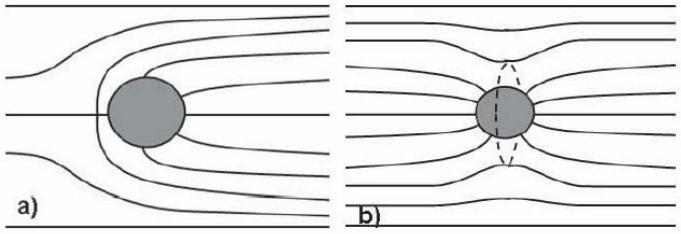

FIG. 1. Schematic illustrations of (a) a dipolar configuration with a hyperbolic hedgehog and (b) a Saturn-ring configuration.

---

*) Adapted from :C. Voeltz, Y. Maeda, Y. Tabe and H. Yokoyama, Phys. Rev. Lett. **97,** 227801 (2006).

together at the center to fix the gap at ca. 900 _m, while keeping the periphery open for bubble injection. Air bubbles are injected through a heat drawn microaperture of a 100 μm diameter quartz capillary (Moritex) connected to an air pump; see Fig. 2. The capillary tip is pulled over a gas burner or in a laser capillary puller (Sutter Instrument, Model P-200), and its aperture diameter can be controlled between 1 and 20 μm. The injection of uniform air bubbles is achieved by creating a constant relative motion between the capillary tip and the liquid crystal between 5 and 40 cm/s, realized by constant rotation of the sandwich cell. The air flow through the capillary is controlled by varying the capillary length l at a constant pressure difference Δp according to Hagen-Poiseuille's law, indicating that the flow rate is proportional to $\Delta p / l$. After the injection of the air, the sandwich cell is put into a custom-built high-pressure chamber which is connected via a pressure regulator to a nitrogen bottle and which allows the application of high pressure of up to about 1 MPa. The pressure chamber has a sapphire glass (diameter 40 mm, thickness 6.5 mm) as an optical viewport. The textures are observed with an optical microscope (Olympus BX50) in transmission mode. For the analysis of the director configuration, crossed polarizers are employed, whereas for the analysis of the dynamics of the bubble size, the polarizers are omitted for a better resolution of the particle size.

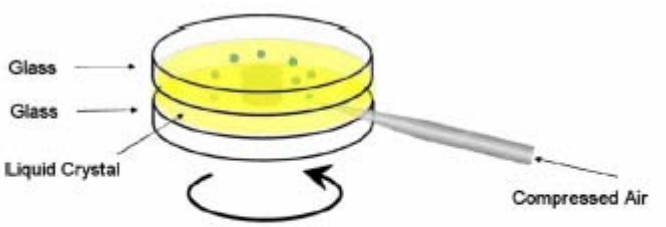

FIG. 2 (color online). Experimental setup: Gas bubbles are injected through a capillary into the liquid crystal which is contained in a rotating sandwich cell.

Because of their buoyancy, the injected air bubbles gradually rise to the top of the sandwich cell. Since the alignment of the nematic director is planar at the glass substrates, and at the bubble surface the anchoring is homeotropic, the air bubbles never directly touch the glass substrates. Figure 3 shows densely packed air bubbles in the nematic matrix. Inside the pressure chamber, the size of the gas bubbles is continuously decreased by applying high pressure to the sample. Figure 4 shows the change of the bubble size by increasing the pressure. In general, by using this pressure technique up to about 650 kPa, a change in bubble size by a factor of 2 can be accomplished.

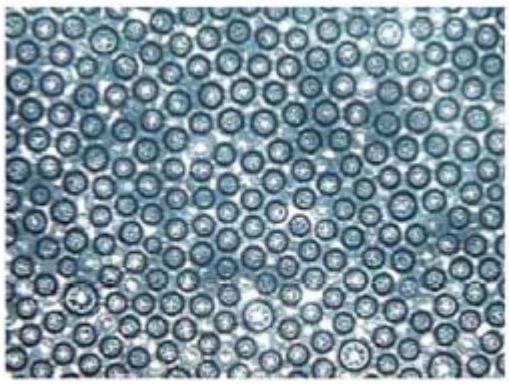

FIG. 3 (color online). Air bubbles in the liquid crystal matrix. The width of the image is 1.75 mm.

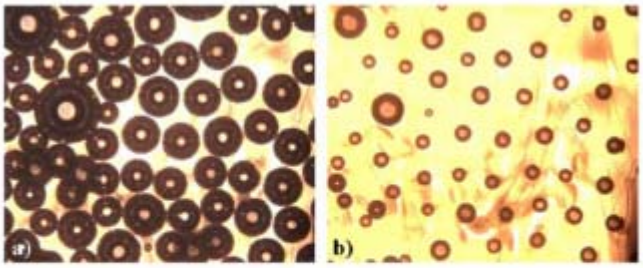

FIG. 4 (color online). Control of bubble size using the pressure technique. Gas bubbles at (a) 100 and (b) 640 kPa. The width of the images is 1.57 mm.

When furthermore utilizing the dissolution of the gas into the liquid crystal, even smaller bubbles can be obtained until the bubbles can be forced to completely disappear. The dynamics of the growing and shrinking of the bubbles by pressure-induced compression as well as by the absorption of air into the liquid crystal has been investigated in more detail, and the radius of an air bubble has been measured under different pressure conditions. Figure 5 shows the change of the bubble radius on applying and releasing pressure. When the pressure is applied, a sudden decrease in the bubble size can be observed due to the compression of the air in the bubbles. On a longer time scale, a further decrease in bubble size is observed, which is due to the absorption of the gas into the liquid crystal. In the same way, after releasing the pressure, first a sudden increase in bubble size occurs and then on a longer time scale follows a slow increase of bubble diameter, which is due to the transport of air from the liquid crystal into the bubble. Therefore, the shrinking process of the bubble can be divided into two regions; see Fig. 6: Region I corresponds to the first rapid decrease in the bubble size due tothe compression of the air. The second region corresponds to the slower shrinking of the bubble due to the absorption of air into the liquid crystal. For region I, the compression of the air bubble should satisfy $P_s R_s^3 / R^3 = 2\gamma / R + P_{out}$, where P_s is an arbitrarily chosen standard pressure, R_s is the bubble radius at this standard pressure, *R* is the radius, and P_{out} is the outside pressure, which follows by combining the Young-Laplace equation and the equation of state of the ideal gas. With the use of a typical surface tension value of $\gamma = 30\text{mN/m}$ [21] and a pressure change between 100 and 500 kPa, the compression of the air gives a shrinking of the bubble radius from 35 to $20.45\mu\text{m}$. This estimate is in good agreement with the experimentally observed compression in region I in Fig. 6. For region II, the absorption of the air into the liquid crystal yields the growth or shrinking rate of the bubble at a constant external pressure P_{out} as

$$\frac{dR}{dt} = -\kappa \frac{2\gamma + R(P_{out} - P_a)}{4\gamma + 3P_{out}R} \qquad (1)$$

where κ is the coefficient of gas

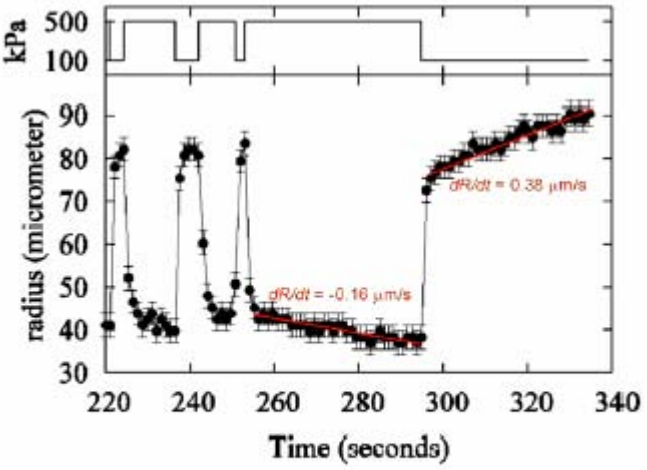

FIG. 5 (color online). Change of bubble radius (bottom graph) by applying and releasing high pressure (change between 100 and 500 kPa, top graph).

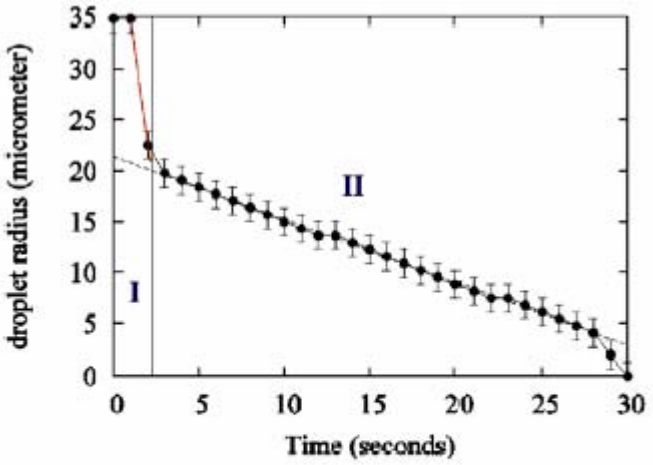

FIG. 6 (color online). Two distinct regions of the shrinking of the air bubble: Compression of the bubble by high pressure (region I) and shrinking of the bubble due to the absorption of the air into the liquid crystal (region II). The external pressure made a jump from 100 to 500 kPa in region I and was kept constant throughout region II.

absorption-desorption rate for unit area and unit pressure, and P_a is the saturated gas pressure in equilibrium with the gas-liquid crystal mixtureacross a plane interface. Equation (1) is reached by combining the Young-Laplace equation and the kinetic expression of Henry's law $dN/dt = -4\pi R^2 k'(P_{in} - P_a)$, where $N = (4\pi/3k_BT)R^3P_{in}$ is the total number of molecules in the bubble as derived from the equation of state, and $k' = 3k_BT\kappa$ is a rate constant. When the internal pressure of a bubble is equal to P_a, while satisfying the mechanical equilibrium with the external pressure P_{out}, the bubble should be in mechanochemical equilibrium with the gas-liquid crystal mixture, corresponding to $dR/dt = 0$ or, equivalently, $R = 2\gamma/(P_a - P_{out})$ in Eq. (1). One should note that this is an unstable equilibrium: Bubbles smaller than this *R* further shrink and those bigger than *R* should further grow.

Equation (1) involves only one characteristic length scale $R_c = \gamma/P_{out}$. For a typical surface tension value of $\gamma = 30\text{mN/m}$ and $P_{out} = 300\text{kPa}$, we obtain $R_c = 0.1\mu\text{m}$. When the bubble radius *R* is sufficiently large so that $R >> R_c$, the shrink/growth rate of the bubble becomes constant at $-\kappa(1 - P_a/P_{out})/3$, as long as $|P_a/P_{out} - 1|$ is not too small compared to unity. Since the bubbles we examined here are larger than $1\mu\text{m}$, we expect this linear growth and shrink behavior to hold. The results shown in Figs. 5–7 indicate that this is really the case. From the two slopes dR/dt in Fig. 5 for shrink (500 kPa) and growth (100 kPa) processes, we find $P_a = 230.1\text{kPa}$ and $\kappa = 0.88\mu\text{m/s}$. In a separate run of experiment (data not shown), the absorption rates are obtained for two different applied pressures on two fresh samples (no prior absorption of air). From these data, κ and the saturation pressure P_a are independently obtained as $\kappa = 0.84\mu\text{m/s}$ and $P_a = 300\text{kPa}$. Although the linear growth and shrink behaviors are well followed in all of the experiments we conducted so far, the absolute value of the rate exhibited a significant variation up to 100% even in the same specimen, depending on the point in the cell. This is probably due to the inhomogeneous degree of saturation, leading to the nonuniform distribution of P_a. Using the high-pressure technique to control the bubble size, we are able to test the theoretical prediction of the particle-size-induced configurational transition. We made a polarizing microscopic observation of shrinking bubbles with the background alignment

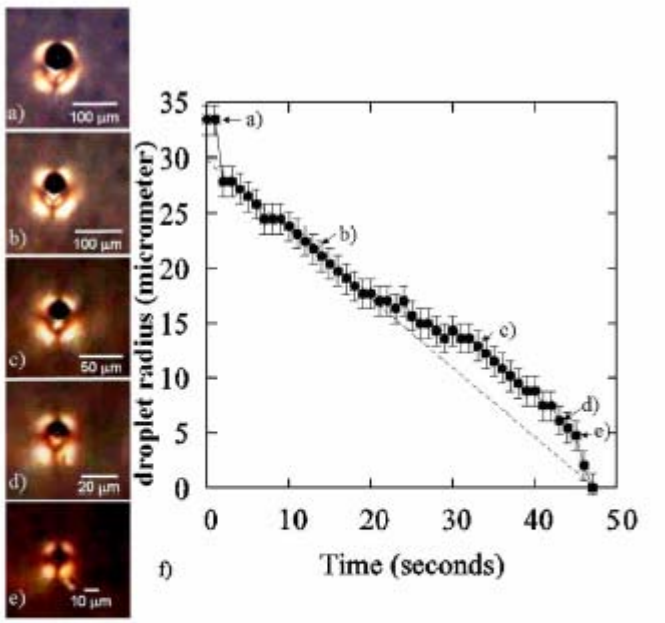

FIG. 7 (color online). (a)–(e) Inducing a transition from a dipolar hyperbolic hedgehog configuration [(a)–(d)] to a quadrupolar Saturn-ring configuration [(e)] by decreasing the radius of the gas inclusion. 500 kPa (initial pressure 100 kPa) is applied in order to induce the shrinking of the bubble size. (f) Bubble radius as a function of time.

direction parallel to the optic axis of crossed polarizers to have the best visibility of the distorted cloud around a bubble (Fig. 7). Choosing a single, well-isolated bubble with a dipolar configuration, we monitored the configuration variation as the bubble size was decreased under a high pressure. As shown in Figs. 7(a)–7(e), at an *apparent* radius close to $5\mu\mathrm{m}$ on shrinking, an abrupt change of view takes place from the asymmetric dipolar state to a symmetric profile featured with a dark cross. Although we do not have direct evidence for the Saturn ring itself, the symmetrical profile is a clear reminiscence of the quadrupolar structure. Figure 7(f) shows the bubble radius as a function of time, when the pressure is increased from 100 to 500 kPa for the transition shown in Figs. 7(a)–7(e). The apparent bubble radius at which the transition occurs, according to Fig. 7, is about $5\mu\mathrm{m}$. This value is likely to be an overestimate due to the limited resolution of the polarizing microscopy. If we interpolate between the vanishing point of t =47 s and the initial region before t =20 s on the basis of the theoretical linear relation, we obtain the lower bound for the bubble radius at the con-figuration transition to be $1\mu\mathrm{m}$ [see Fig. 7(f)]. The real bubble size should lie between these two boundaries. Since there are a number of sources of uncertainties such as the surface tension variation as a result of surface active contaminants and the insufficient optical resolution, the rather big range of possible bubble size may be tolerable. The relative energetic stability of the Saturn-ring and hyperbolic hedgehog configurations has been investigated by a numerical scheme based on the Landau–de Gennes formalism [22]. The total free energy of the system is basically proportional to the radius R of the colloidal particle for both the Saturn-ring and hedgehog configurations. For the Saturn-ring case, however, the -1/2 disclination line surrounding the particle makes a non-negligible contribution in the form of $R\ln R/\xi$, with ξ being the coherence length of the nematic orientational order. This logarithmic contribution is indeed responsible for the hyperbolic hedgehog–Saturn-ring transition. The numerical study in Ref. [22] has shown that the equilibrium transition point is approximately located at 160ξ: By employing $\xi = 10\mathrm{nm}$ as a typical value, we obtain $1.6\mu\mathrm{m}$ for the transition radius. In view of possible hysteresis, the real transition should take place at a radius smaller than this value. As is usual for such a continuum theoretic estimate, the present level of agreement between the experimental result and the theory seems satisfactory.

To conclude, we developed a high-pressure technique that allows the simultaneous observation of the director configuration around a single bubble, while its size is continuously changed. When the size of the bubble is decreased by the applied pressure, a transition from a hyperbolic hedgehog configuration (dipole) to a Saturnring configuration (quadrupole) occurs, as has been predicted theoretically.

[1] O.V. Kuksenok, R.W. Ruhwandl, S.V. Shiyanovskii, and E. M. Terentjev, Phys. Rev. E **54**, 5198 (1996).

[2] T. C. Lubensky, D. Pettey, N. Currier, and H. Stark, Phys. Rev. E **57**, 610 (1998).

[3] B. I. Lev and P. M. Tomchuk, Phys. Rev. E **59**, 591 (1999).

[4] H. Stark, Eur. Phys. J. B **10**, 311 (1999); Phys. Rep. **351**, 387 (2001).

[5] J. Fukuda, H. Stark, M. Yoneya, and H. Yokoyama, Phys. Rev. E **69**, 041706 (2004).

[6] K. Kocevar and I. Musevic, Phys. Rev. E **65**, 021703(2002).

[7] I. Musevic, M. Skarabot, U. Tkalec, M. Ravnik, and S. Zumer, Science **313**, 954 (2006).

[8] M. Yada, J. Yamamoto, and H. Yokoyama, Phys. Rev. Lett. **92**, 185501 (2004).

[9] I. I. Smalyukh, O. D. Lavrentovic, A. N. Kuzmin, A.V. Kachynski, and P. N. Prasad, Phys. Rev. Lett. **95**, 157801 (2005).

[10] T. Yamamoto, J. Yamamoto, B. I. Lev, and H. Yokoyama, Appl. Phys. Lett. **81**, 2187 (2002).

[11] P. Poulin, H. Stark, T. C. Lubensky, and D. A. Weitz, Science **275**, 1770 (1997).

[12] P. Poulin, V. Cabuil, and D. A. Weitz, Phys. Rev. Lett. **79**,4862 (1997).

[13] P. Poulin and D. A. Weitz, Phys. Rev. E **57**, 626 (1998).

[14] O. Mondain-Monval, J. C. Dedieu, T. Gulik-Krzywicki, and P. Poulin, Eur. Phys. J. B **12**, 167 (1999).

[15] Y. Gu and N. L. Abbott, Phys. Rev. Lett. **85**, 4719 (2000).

[16] E. M. Terentjev, Phys. Rev. E **51**, 1330 (1995).

[17] R.W. Ruhwandl and E. M. Terentjev, Phys. Rev. E **55**,2958 (1997).

[18] D. Andrienko, G. Germano, and M. P. Allen, Phys. Rev. E **63**, 041701 (2001).

[19] It has been demonstrated that an intense electric field can induce a similar transition from the hedgehog to the Saturn-ring configuration [20]. The underlying mechanism, however, is the destabilization of the hedgehog defect under the electric field and, hence, is qualitatively different from that under consideration in this Letter.

[20] J. C. Loudet and P. Poulin, Phys. Rev. Lett. **87**, 165503 (2001).

[21] M. G. J. Gannon and T. E. Faber, Philos. Mag. A **37**, 117(1978).

[22] J. Fukuda, M. Yoneya, and H. Yokoyama, Eur. Phys. J. E **13**, 87 (2004).